Physica B: Condensed Matter 566 (2019) 6–16

Contents lists available at ScienceDirect

Physica B: Condensed Matter

journal homepage: www.elsevier.com/locate/physb

Fabrication of heterojunction diode using doped-poly (ortho-aminophenol) for solar cells applications

A.F. Al-Hossainy[a,b], M. Sh. Zoromba[c,d,*], M.H. Abdel-Aziz[c,e], M. Bassyouni[f,g], A. Attar[h], M. Zwawi[h], A.A.I. Abd-Elmageed[i], H.A. Maddah[c], A. Ben Slimane[b,j]

[a] Chemistry Department, Faculty of Science, New Valley University, 72511, Al-Wadi Al-Gadid, Al-Kharga, Egypt
[b] Chemistry Department, Faculty of Science, Northern Border University, Arar, 1321, Saudi Arabia
[c] Chemical and Materials Engineering Department, King Abdulaziz University, Rabigh, 21911, Saudi Arabia
[d] Chemistry Department, Faculty of Science, Port-Said University, 42521, Port-Said, Egypt
[e] Chemical Engineering Department, Faculty of Engineering, Alexandria University, Alexandria, Egypt
[f] Department of Chemical Engineering, Faculty of Engineering, Port Said University, Egypt
[g] University of Science and Technology, Materials Science Program, Zewail City of Science and Technology, October Gardens, 6th of October, Giza, 12578, Egypt
[h] Mechanical Engineering Department, King Abdulaziz University, Rabigh, 21911, Saudi Arabia
[i] Physics Department, Faculty of Science, New Valley University, 72511, Al-Wadi Al-Gadid, Al-Kharga, Egypt
[j] Chemistry Department, Faculty of Science, Gafsa University, Tunisia, 1089, Tunisia

ARTICLE INFO

Keywords:
Doped-poly (o-aminophenol)
Optical and electrical properties
Polymer solar cell

ABSTRACT

Hydrochloric acid doped poly ortho aminophenol (POAP) is prepared in a high acidic medium (pH ~ 0.6) using $FeCl_3$ as an oxidizing agent. The polymerization process is conducted in the presence of polyethylene glycol (PEG200) as a soft template at 25 °C. The method pertains to the reduction of $FeCl_3$ by *o*-amino phenol (OAP) at room temperature. The obtained POAP polymer is soluble in common organic solvents such as dimethylformamide and chloroform. The resulting POAP is investigated by various analyzing techniques including Fourier transform infrared (FT-IR), X-ray diffraction (XRD), proton nuclear magnetic resonance (^{1}HNMR), and scanning electron microscope (SEM). The analysis revealed that both quinoid and benzoid structures are existing in the polymer backbone. POAP thin film is fabricated and its optical properties are also investigated. Au/POAP/TiO_2/p-Si/Al heterojunction solar cell is fabricated as well. The resulting average value of power conversion efficiency (PCE) of Au/POAP/TiO_2/p-Si/Al heterojunction solar cell is found to be 4.28%.

1. Introduction

Recently, a wide interest in the process of amino phenol polymerization has appeared, whether o, m-, or p-amino phenol [1–8]. This interest is due to the important applications of aminophenol polymerization products in various areas, such as electrochemical sensors, electrocatalysis, and bioelectrocatalysis. Previous studies have dealt with aminophenol polymerization by chemical oxidation using different oxidizing agents, such as hydrogen peroxide [1], ammonium persulphate [2–5], copper bromide [6] and potassium dichromate [7], the use of different oxidizing agents at different pH values led to differences in physical properties of the resulting polymers.

Poly (ortho-aminophenol) belongs to conjugated polymers class which interact with light, and is obtained by polymerization of ortho-aminophenol, its properties depends on the reaction conditions. Polymerization in acidic solutions leads to creation of poly(ortho-aminophenol) with a phenoxazine unit which has great pharmacological and industrial utility [8].

There are some applications that require improved physical properties of polymers, such as electrical conductivity. The electrical conductivity of polymers can be improved by utilizing a relatively small amounts of a dopant which raises the conductivity and converts low or non-conducting polymer to a semiconducting polymer [9,10]. The doping process varies according to the nature of the polymer as it is in the conjugated polymers where redox doping are used, including donation of electron to a -conjugated system (n-type) or withdrawing of electron from a conjugated system (p-type) [11]. Numerous conjugated polymers are also well-organized electron donors and satisfactory hole transporters through their visible-light excitation. Therefore, conjugated polymers owning inorganic semiconductors characteristics are evincing more attention for electronic, photocatalytic, optical, and photoelectric conversion purposes [12,13].

* Corresponding author. Chemical and Materials Engineering Department, King Abdulaziz University, Rabigh, 21911, Saudi Arabia.
E-mail address: mzoromba@kau.edu.sa (M.S. Zoromba).

https://doi.org/10.1016/j.physb.2019.04.030
Received 8 April 2019; Received in revised form 26 April 2019; Accepted 27 April 2019
Available online 29 April 2019

Thin films of semi-conducting conjugated polymers can be manufactured for the purposes mentioned above by different techniques such as spin coating and thermal evaporation [14]. These fabrication techniques are usually applied under definite circumstances by means of wet or dry techniques. The spin coating technique yields a good adherent layer of nanocrystalline thin film with a high degree of homogeneity [15–17].

The purpose of the current research is divided into two parts, the first part is to prepare hydrochloric acid doped poly ortho-aminophenol (POAP) in a high acidic medium (pH ~ 0.6) by using ferric chloride as an oxidizing agent. The polymerization process is carried out in the presence of polyethylene glycol (PEG200) as a soft template at 25 °C. Various analyzing techniques were utilized to characterize the resultant POAP. The second part is to prepare hydrochloric acid doped POAP nanostructured thin film and to investigate its application for the first time as a new hybrid material in Au/POAP/TiO_2/p-Si/Al diode for solar cell applications. To this end electrical conduction mechanisms of the Au/POAP/TiO_2/p-Si/Al diode was studied with its current-voltage characteristics under dark, and at varied temperatures in the range of 298–386 K, also photovoltaic properties of POAP/p-Si heterojunction device under various light intensities in the range of 10.1–20.5 W m^{-2} were studied.

2. Experimental section

2.1. Materials

All chemical reagents were used without additional purification. O-aminophenol (Across Organics: Thermo Fisher Scientific), Polyethylene glycol (PEG200) (Shanghai chemicals), ethanol (Aldrich), anhydrous dimethyl formamide (DMF), Dimethyl sulfoxide (DMSO): Aldrich and anhydrous ferric chloride (Aldrich), Hydrochloric, hydrofluoric, nitric and acetic acids (Aldrich), Single crystal of (p-Si) and perchloric acid ($HClO_4$), Titanium (IV) bis(acetoacetonato) di(isopropanoxylate) (98%) were bought from Sigma-Aldrich.

2.2. Synthesis of hydrochloric acid doped-poly (o-aminophenol) (POAP)

The preparation was conducted at room temperature; typically, 4.36 g o-aminophenol was dissolved in 50 ml ethanol under magnetic stirring at 850 rpm. 3 ml PEG200 was added to ethanolic solution of ortho-amino phenol. Concentrated hydrochloric acid was dropped into the mixture until the pH reached 0.25. 80 ml from aqueous solution of $FeCl_3$ (0.5 M) were added drop by drop to the monomer solution for 3 h. The ratio between monomer and oxidizing agent is 1:1. The pH value for the resulting mixture was recorded and found to be 0.6. The resulting mixture was left overnight at room temperature. The resulting hydrochloric acid doped-poly (o-aminophenol) was filtrated. The washing process of POAP was carried out for several times by using distilled water followed by ethanol to remove any excess of unreacted monomer, oxidizing agent, and PEG200, doped POAP was dried at 60 °C.

2.3. Solar cell fabrication

A spin coating technique (spin coater model 1001 CPSII) was utilized in fabricating the Au/POAP/TiO_2/p-Si/Al diode of 0.3 m^2 typical area. The optical glass substrates were cleaned in a washing machine using deionized water and then heated in an oven at 400 °C for 1 h. The deposited layer (≅200 ± 3 nm) was dried for 48 h in the dark and at room temperature. The spin coating machine was spun at a speed of 1000 rpm for 15 s.

The POAP was then sandwiched between TiO_2 and Au electrodes (TiO_2/P-Si/POAP/Au). On P-Si wafer substrates a compact layer of thickness 100 nm (TiO_2) was deposited by spin coating at room temperature of the forerunner solution, titanium (IV) bis(acetoacetonato) di(isopropanoxylate) diluted in ethanol. Then a smooth p-type single crystal Si wafer with (100) was deposited aligned to its surface with 1.6×10^{23} m^{-3} concentration and 400 μm thickness. TiO_2 is employed as the n-type material in a junction for charge separation and to provide remarkable electron transport characteristics, including a band gap at wavelength shorter than 400 nm [18,19]. The chart of the Au/POAP/TiO_2/p-Si/Al diode configuration is displayed in Fig. 1.

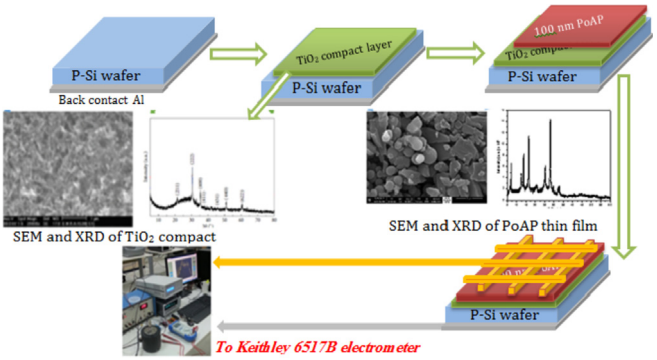

Fig. 1. Chart of the fabrication Au/POAP/TiO_2/p-Si/Al heterojunction diode.

2.4. Characterization

The structure of the POAP was confirmed by using A JEOL RESONANCE- 500 MHz nuclear magnetic resonance (NMR) instrument employing DMSO-d_6 as a solvent, Fourier transform infrared spectroscopy (Thermos Nicolet Model 6700), and X-ray diffraction (XRD).

The structure of the composites was investigated by a Philips X-ray diffractometer (model X' pert) with monochromatic Cu Ka radiation (1.54183 Å) operated at 40 kV and 25 mA. The surface characterization of POAP powder was performed by using (JSM 5800; JEOL SEM) Scanning Electron Microscopy. The conductance of the synthesized POAP thin film was obtained by Keithley four probe nanovoltmeter. The characterization by Cyclic Voltammograms of POAP-modified glassy carbon electrodes in different concentrations of $HClO_4$ electrolyte solution were performed, the optical properties of UV spectrum of poly(o-aminophenol) in the dimethyl sulfoxide and of the poly(o-aminophenol) thin film, and the electrical properties were measured as well. The UV spectra of POAP dissolved in DMSO solvent in 100–1400 nm wavelength were recorded on a spectrometer Perkin-Elmer Lambda 5 UV-VIS-NIR spectra.

3. Results and discussions

3.1. FT-IR analysis

The FT-IR spectrum of the produced doped- poly (*o*-aminophenol) is given in Fig. 2 and the corresponding band assignments are listed in Table 1. The infrared spectrum displayed absorption bands at 3182–3337, 1336–1481, 836–897 and 696–758 cm^{-1}, corresponding to hydroxide group (OH) stretching, bending, rocking and wagging vibrations respectively, due to the presence of water molecules. The two strong peaks at 1674 and 1555 cm^{-1} present the quinoid and benzenoid rings stretching vibrations, respectively. The presence of these two rings in the structure demonstrates that the poly (o-aminophenol) is composed of the amine and imine units. The two bands at 1254 and 1019 cm^{-1} are due to the stretching of the C—O—C (ether linkage), the peak C—O—C equalized stretching vibrations are clearly determined in POAP. The ether linkage confirms that the POAP polymer takes ladder-type structure [3,20,21]. The bands at 953 and 787 cm^{-1} designate the C—H aromatic (out –of-plane bending). Between 1300 and 1400 cm^{-1}, the band at 1374 cm^{-1} can be attributed the stretching vibrations of charge C—N^+ segments (~ indicates the intermediate bond between the

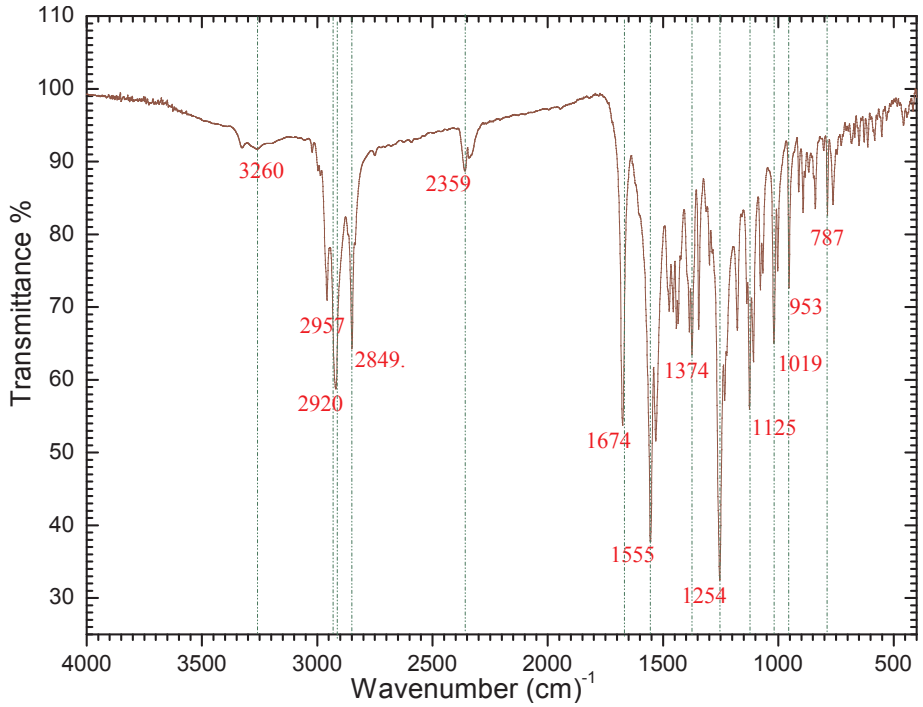

Fig. 2. FT-IR of poly (o-aminophenol) (POAP).

Table 1
Vibrational frequencies and assignments for POAP.

Band (cm^{-1})	Assignment
3260–2000	The stretching of aromatic C—H and —NH stretching
2957	—CH stretching.
1674 and 1555	Quinoid and benzenoid rings stretching vibrations, respectively.
1674	—C=N— in quinonimine units.
1374	C—N stretching vibrations of the second aromatic amine.
1254 and 1019	Stretching of the C—O—C (ether linkage) [5,22]
787	—C—H bending vibration corresponding to ortho-substituted aromatic rings

single and double bonds). The bands are located with the range of 900–600 cm^{-1} related to the C—H bending of an aromatic ring substitution of the POAP. These results concords with previous statement that the poly(o-aminophenol) synthesized contains a condensed phenoxazine ring in its structure. The band at 1125 cm^{-1} is a characteristic of POAP (doped with chloride ion). Besides, the ν(NH) vibration was displayed at 3260 cm^{-1}. This confirms that the polymerization was carried out through the —NH group, in the FT-IR spectrum, supporting the presence of (CH—NH—CH—) functionality in the POAP. The polymerization mechanism of OAP can be suggested as described in the Fig. 3.

3.2. ^1H NMR spectral analysis

Fig. 4 displays the ^1H NMR spectra of the prepared POAP. In this spectrum, the chemical displacement is noticed for two hydrogen atoms belonging to the benzene rings in the regions of 6–8 ppm. A multiplet can be noticed referred to the aromatic protons at 7.4–7.8 δ. The other four positions of the benzene rings are occupied by substituents in the chain of the polymer. Therefore, the peak at δ 10.827 ppm presents the OH proton belonging to the H_2O molecules exist in the polymer [23]. The peak at δ 7.791 ppm is attributed to —NH— present in the polymer backbone [24]. Two peaks were detected at 2.491 ppm and at 3.347 ppm corresponding respectively to the protons of $-CH_3$ group of DMSO and to the protons which are existing in the residue water molecule in the polymer besides in the solvent. These results from ^1H NMR spectra agree with the results provided by the FT-IR spectra mainly concerning the NH and OH groups.

3.3. Surface morphology study

The surface morphology of the POAP powder was scanned by SEM as shown in Fig. 5. The POAP is located in microstructure. The poly (o-aminophenol) exhibits polydisperse and smooth particles at high magnification (×30,000) with particles in the 3 μm size range at 20.00 kV.

Fig. 5 showed the morphology of top surface of doped POAP powder. POAP polymer had a distorted spherical-like but also had some differences in the surface and skin layer morphologies. The size of the doped POAP polymer microstructure displays a magnificently discrete microscale polymer film. The resulting microparticles have a regular plate-like shape with an average diameter range of 0.79 mm. These microparticles are produced from the agglomeration of around 20–35 crystallites (Image J software program) [25].

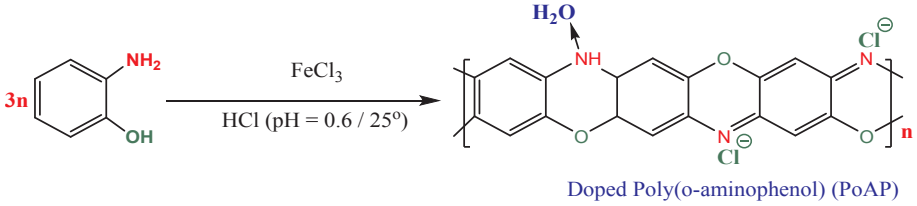

Fig. 3. Suggested scheme for polymerization of o-aminophenol (OAP) monomer.

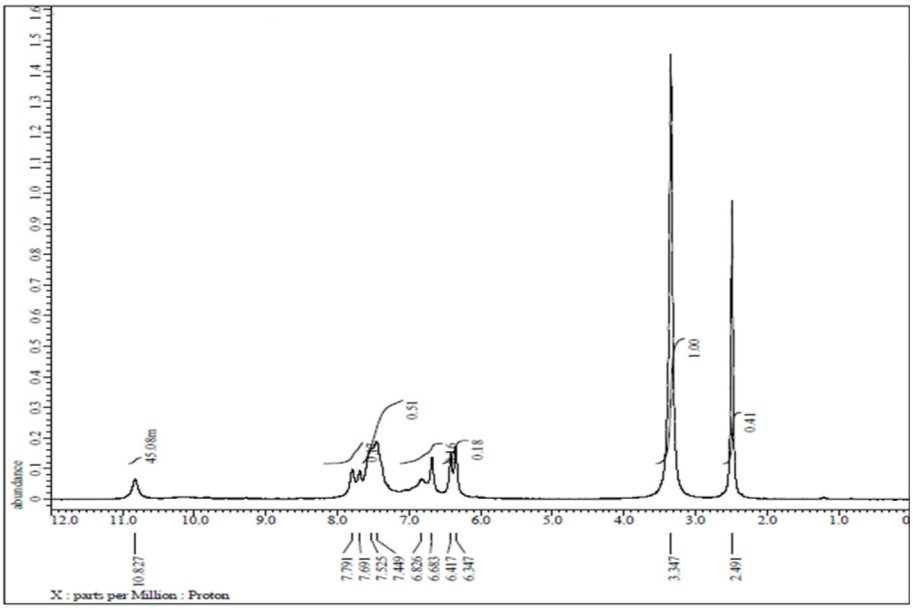

Fig. 4. ^{1}HNMR spectra of poly (o-aminophenol).

3.4. X-ray diffraction

Fig. 6 illustrates the XRD pattern of Au/POAP/TiO_2/p-Si/Al 100 nm thin film thickness. The existence of many diffraction peaks with varied intensities on the spectrum is noticed, and it reveals that the thin film form is of a polycrystalline nature. The crystallinity and orientation of conducting polymers are very interesting, due to the higher metallic conductive state engendered by a more highly ordered system [26]. This organization inside the polymer is displayed by the existence of reasonably sharp peaks. The morphology of the polymer is also described by the Bragg's peaks (2θ) location. The polymer exhibits the strongest peaks at 7.02°, 13.70°, 16.44°, 17.66°, 25° and 28.04°. These broad peaks are a sign of the crystalline domains in the amorphous structure of POAP. 2θ = 28.04° reports the Van Der Waals distances among layers of phenylene rings of the poly aminophenol. The good level of crystallinity and the ordered structure in POAP may be attributed to the hydrogen bonding intrachain linkage and electrostatic (van der Waals) interactions through amine and/or phenolic group found in the polymer [27,28]. Fig. 6 exhibits that the scattering of the peaks proves the formation of Au/POAP/TiO_2/p-Si/Al complex with well-known crystallinity. The full width of the peak at half-maximum intensity (FWHM) of the largest three signals allows to determine the crystallite size (D) of the Au/POAP/TiO_2/p-Si/Al complex; at 2θ = 13.70°, 16.44° and at 28.04°. The average value of the crystallite dimension (D) was 22.84 nm. The interplaner spacing d was calculated by utilizing Debye-Scherrer method and applying Bragg's relation and the mean value of d was 5.171 Å. Peak analyzer information (Fitting data) of POAP as-deposited thin film are shown in Table 2.

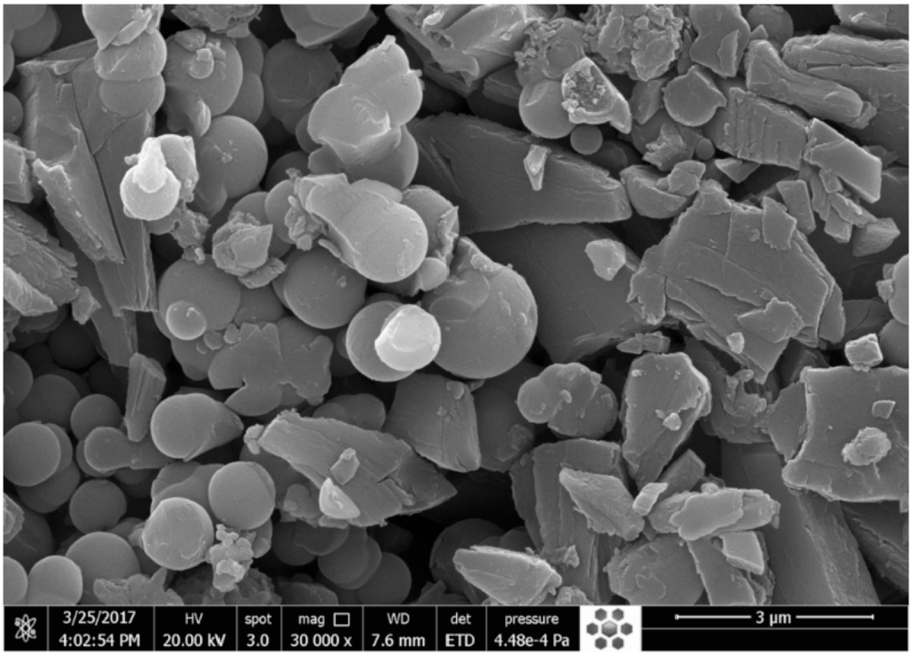

Fig. 5. SEM of doped poly (o-aminophenol) (POAP) powder.

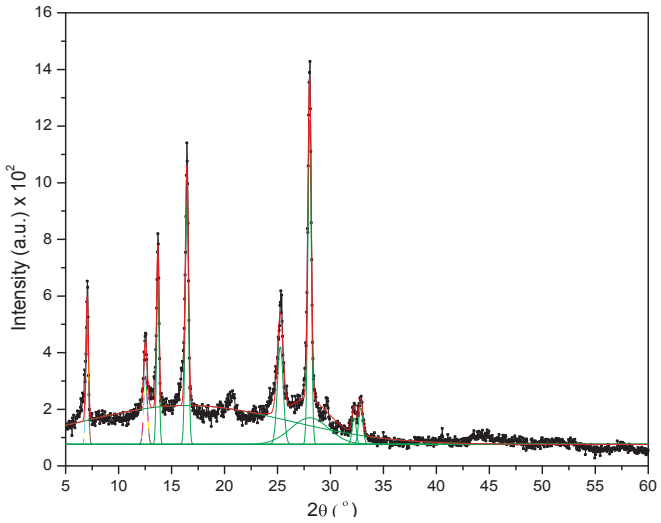

Fig. 6. Fitting peaks of X- ray diffraction pattern of Au/POAP/TiO_2/p-Si/Al thin film.

Table 2
Peak analyzer (Fitting data) of POAP as-deposited thin film.

No	Area	Center	Width	Height	FWHM	D (nm)	d-spacing
1	131.24	7.02	0.238	440.63	0.280	28.470	12.582
2	108.24	12.54	0.357	242.23	0.420	19.055	7.052
3	176.76	13.71	0.245	576.29	0.290	27.792	6.455
4	321.91	16.44	0.303	847.57	0.360	22.515	5.390
5	403.83	17.67	0.235	144.082	0.221	36.443	5.017
6	261.02	25.27	0.599	347.614	0.705	11.551	3.523
7	529.08	28.035	0.357	1182.21	0.420	19.492	3.18
8	30.281	29.67	0.326	74.191	0.383	21.450	3.011
9	32.321	32.24	0.324	79.621	0.381	21.702	2.775
10	49.73	32.86	0.353	112.413	0.416	19.950	2.723
Average	567.74	21.54	0.337	404.685	0.390	22.842	5.171

3.5. Optical properties

Fig. 7 displays UV–vis spectrum of POAP solution in DMSO (0.025 g/10 ml) and POAP thin film onto glass substrate, two different types of curves were distinguished. The first curve with various maximum wavelengths characterizes the POAP thin film: A max a.u (λ nm) 360 (3.05), 670 (1.33), 730 (1.31), 990 (0.239) and 1210 (0.136). In case of POAP solution in DMSO, the spectrum UV contains just the following peaks: A max a.u (λ nm) 320 (3.57), 695 (0.869). Two major absorption peaks in the spectra were detected; the initial peak at 320 nm (3.57 eV) is related to the $\pi - \pi*$ transition of the phenyl rings derived from the extent of conjugation between them in the polymer. While $n-\pi*$ transition among the HOMO orbital of the benzenoid ring and the LUMO orbital of the quinoid ring is represented by the next absorption peak at 695 nm. It is sensitive to the whole oxidation state of the polymer [29]. The signal placed at 320 nm is more intense than that placed at 695 nm indicating a higher oxidation of the o-aminophenol to obtain the polymer. In the second spectra characterizing the POAP thin film, 5 signals were recorded: the value of the wavelength and highest intensity signal placed at (360 nm, 3.05) and a second region containing 4 weak transitions in the range between 600 nm and 1300 nm placed in 670(1.33), 730 (1.31), 990 (0.239) and 1210 (0.136), individually. This section of the spectra comprises of the Q band, the sort and the location of substituents on the rings change extremely the strength of Q bands. Thus, there is a variation in the signal strengths of the Q bands with π-electrons, as vinyl groups, attached straight to the α-positions. In addition, the bands patters of the Q bands are affected by the protonation or by coordination with any metal by the macrocycles [30,31]. As observed, Au/POAP/TiO_2/p-Si/Al exhibits one split signal. The higher intensity peak corresponds to the high-energy side peak. π-π* excitation among bonding and antibonding molecular orbitals provide definite categorized peaks for Au/POAP/TiO_2/p-Si/Al film in the visible region (Q-band) at 670 and 730 nm [32–35]. On the other side, the other signal with low-energy of the Q-band is interpreted, as a second π-π* transition.

Bardeen et al. [36] gave a way to elucidate the transition, the fundamental absorption edge within the one electron theory. The following equation expresses the relation between the absorption coefficient α

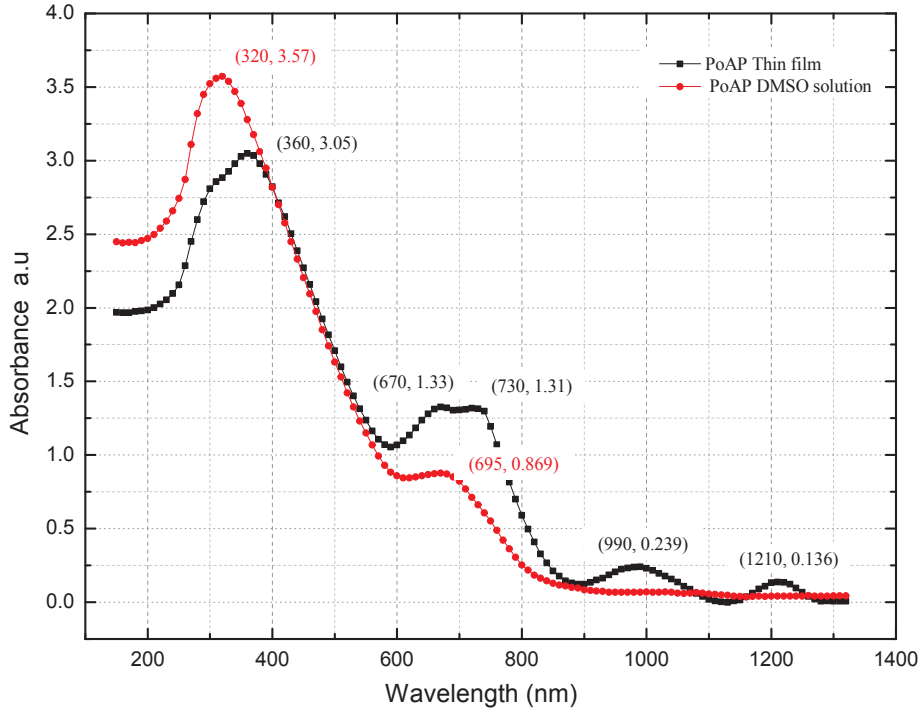

Fig. 7. UV–vis spectrum of POAP solution in DMSO and POAP thin film.

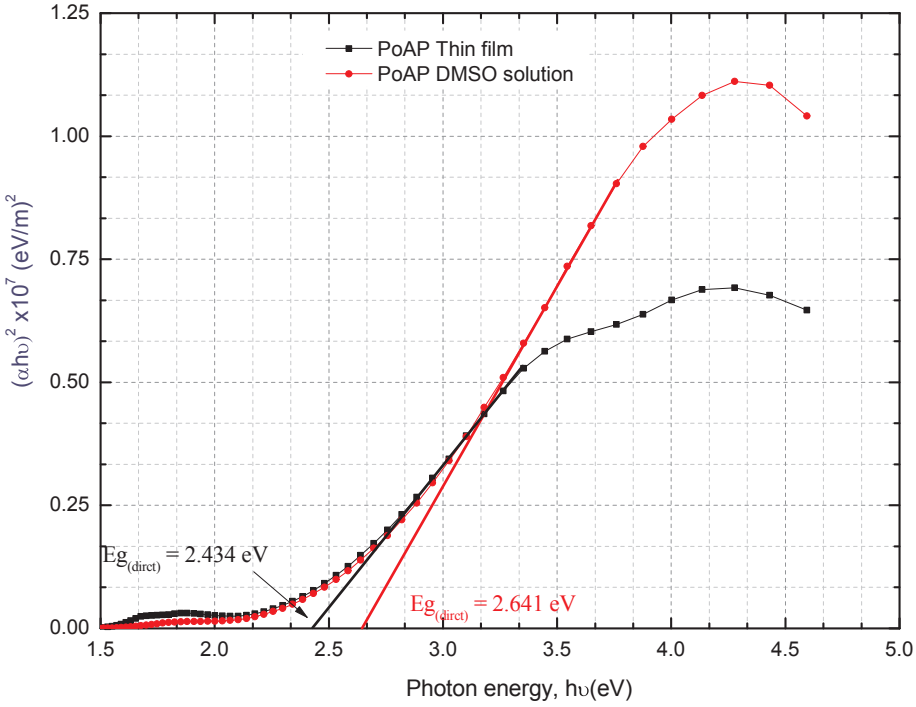

Fig. 8. Variation of (α hν)^2 × 10^7 versus photon energy hν (eV), for POAP solution in DMSO and POAP thin film.

and the photon energy

$$(h\nu)\ \alpha = \alpha_o(h\nu - E_g)^X \quad (1)$$

For direct allowed transitions x = 1/2 and for direct forbidden transitions x = 3/2, respectively. For indirect allowed transitions x = 2 and for indirect forbidden transitions x = 3, respectively. For a direct allowed transition E_g is the optical band gap and α_o is a constant [36–38]. Plotting $(\alpha h\nu)^2$ versus hν above the absorption edge yields straight lines as shown in Fig. 8. The energy gaps are 2.454 eV and 2.641 eV for POAP thin film and POAP solution in DMSO, respectively. To obtain optical band gap the linear portion of the plot to $(ah\nu)^2 = 0$ is extrapolated.

3.6. Electrical properties

3.6.1. Dark current–voltage characteristics

Fig. 9 describes the variation of dark current versus voltage for Au/POAP/TiO_2/p-Si/Al heterojunction diode operated at different temperatures. The curves in the diagram explain the solar cell-like behavior, as well as with the forward and reverse direction. The presence of p^- p+ heterojunction can explain this behavior. The barrier at the interface with p^- p+ heterojunction, where the built-in potential is developed, limits the forward and reverse carrier's flows across the junction. At low voltage range the forward current increases with applied voltage for the junction. This increase was assigned to the presence of the depletion region between P-Si and POAP film. An increase of current with temperature is reported for the same applied voltage, this is interpreted by a negative temperature coefficient resistivity. Moreover, the rectification ratio RR, considering as the ratio of the forward current to the reverse current at a certain applied voltage, i.e. RR = $(I_F/I_R)_\upsilon$ = constant (The value of the rectification ratio is about 60 at a bias potential of 2.04 V).

The characteristics behavior measured experimentally for non-ideal diode, is generally more complex than that of the ideal diode. This fact is explained by the presence of various conduction mechanisms. To pattern the eventual and likely conduction mechanisms, the following expression is frequently used [38]:

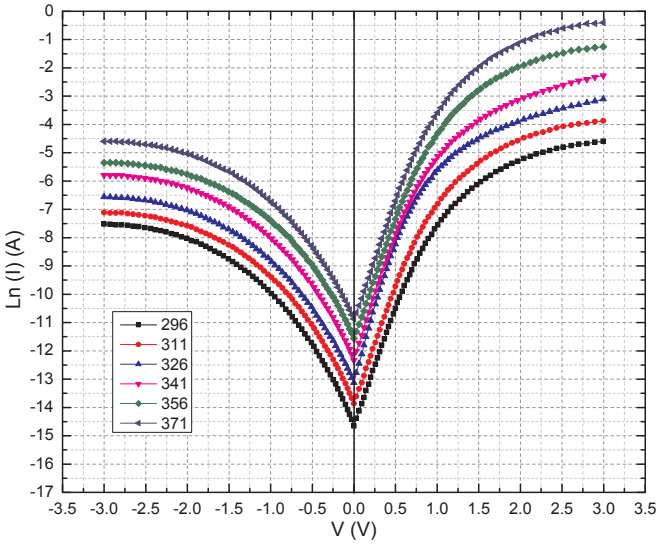

Fig. 9. Evolution of dark current versus voltage for Au/POAP/TiO_2/p-Si/Al heterojunction diode.

$$I = I_{01}[exp\frac{q(V - IR_s)}{n_1K_BT} - 1] + I_{02}[exp\frac{q(V - IR_s)}{n_2K_BT} - 1] + \frac{V - IR_s}{R_{sh}} \quad (2)$$

The action of parasitic series and parallel resistance present in this equation can obfuscate the intrinsic parameters of the apparatus. However, the plot of (R_J) versus voltage provides R_s and R_{sh}. R_J is expressed by $R_J = \partial V/\partial I$, and is provided from the curves. It is noticed that R_J reaches a constant value of 452 at high forward bias potentials. In a high reverse bias potential, the junction resistance reaches a maximum value of 21.79 kΩ. The cause of this shunt resistance could be a likely local harm of the junction and/or probable waste currents at the edges of the apparatus.

The ideality factor (n) has a great influence on the precision of the temperature value. The apparent measured temperature will change with modifying the diode ideality factor. If a remote diode sensor with a

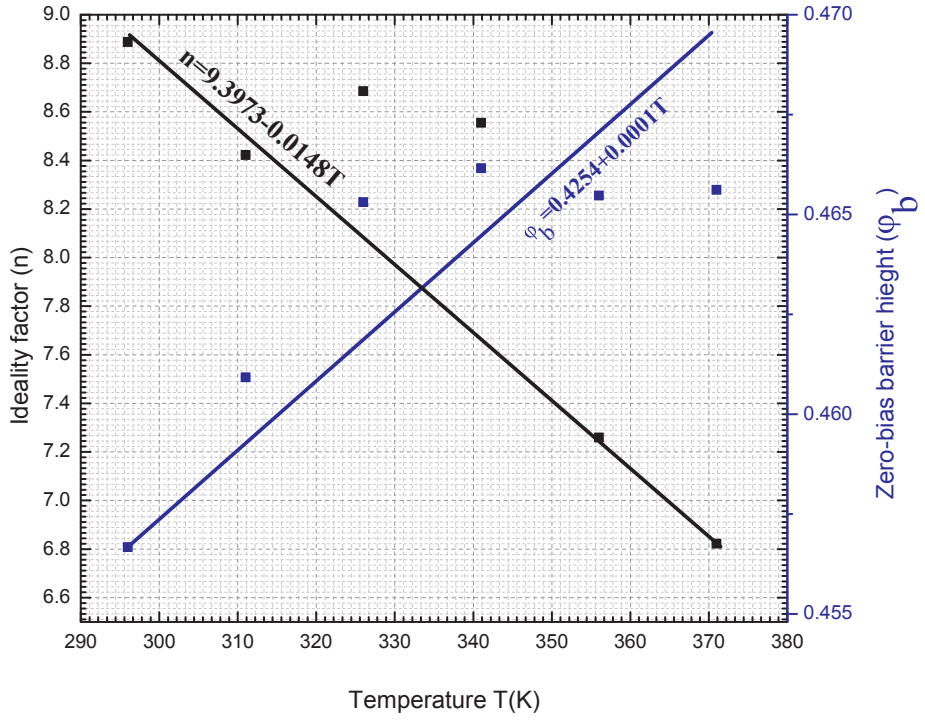

Fig. 10. Variation of the ideality factor versus temperature for Au/POAP/TiO_2/p-Si/A heterojunction diode.

nominal ideality factor, $n_{Nominal}$, is used to display the temperature of a diode with a different values of n $_{Actual}$ the following expression was used in order to correct differences in ideality factor:

$$T_{Actual} = T_{Measured}\, x \frac{n_{Nominal}}{n_{Actual}} \tag{3}$$

and the following relation:

$$n_b = 16.963 - 0.0266\ T \tag{4}$$

Further analysis was executed to verify that the thermionic emission is the operating conduction mechanism. According to the thermionic conduction, the saturation current was calculated from the following equation [39].

$$I_{01} \alpha T^2 exp(-\frac{e\varphi_b}{k_B T}) \tag{5}$$

The thermionic mechanism was confirmed by the straight line, which acquired from the curve giving the variety of T against φ_b. Fig. 10 indicates that the values of φ_b relating to the complex Au/POAP/TiO_2/p-Si/Al heterojunction diode increase linearly with the temperature. This increasing of φ_b with T is confirmed by the following relation:

$$\varphi_b = 0.4258 + 3 \times 10^{-4} T \tag{6}$$

Another mechanism occurs in the range of forward voltage: −2 V–1.1 V. According to the Fig. 11, the current follows a relation of the form $I \sim V^m$. The slope of the curve ln(I) vs. ln(V) is approximately 3, explaining that the forward biased current is space-charge-limited current (SCLC) commanded by a single dominating trap level. To confirm this result, isolate SCLC measurements were conducted for specimens like Au/POAP/TiO_2/p-Si/Al and it is under processing with other studies. I–V parameters of Au/POAP/p-Si/Al heterojunction solar cell are tabulated in Table 3.

The I–V characteristics under reverse bias for the Au/POAP/TiO_2/p-Si/Al diode in the temperature range 296–371 K are presented in Fig. 12. The plot is under the form of natural logarihmic plot of (ln I) vs. ($V^{0.5}$). The current under a reverse bias, is lower compared to the forward bias. The Schottky effect or the Poole–Frenkel effect and the dark

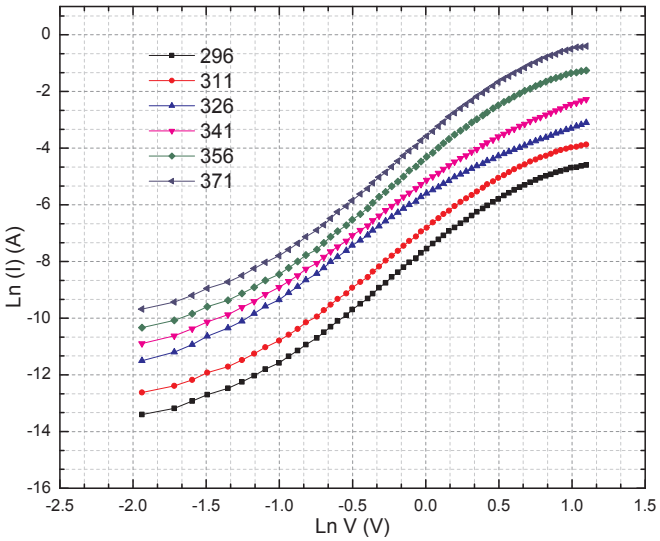

Fig. 11. Variation of current versus the potential for Au/POAP/TiO_2/p-Si/Al heterojunction diode.

Table 3
I–V parameters of Au/POAP/p-Si/Al heterojunction solar cell.

T, K	KT/Q	n	I_o x 10^{-7}	φ_b
296	0.0255	8.888	4.300	0.457
311	0.0268	8.422	9.600	0.461
326	0.0281	8.685	19.90	0.465
341	0.0294	8.555	43.80	0.466
356	0.0307	7.259	95.20	0.465
371	0.0319	6.822	190.0	0.466

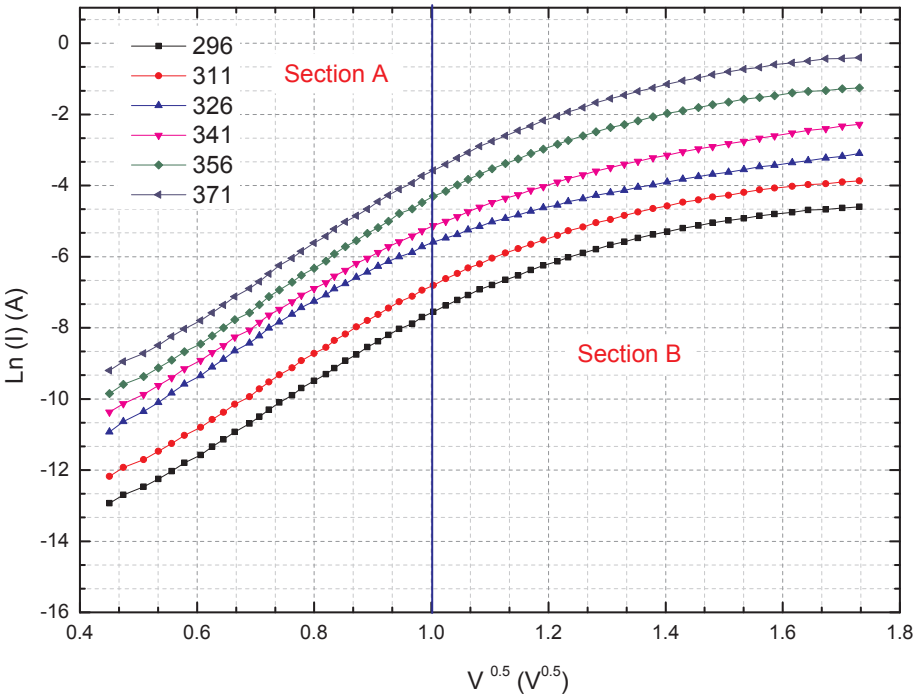

Fig. 12. Reverse bias ln (I) versus $V^{0.5}$ characteristics for the Au/POAP/TiO_2/p-Si/Al heterojunction diodes in the temperature range 296–371 K.

I–V expressions for these processes can explain the presence of distinct regions in the diagram, and expressed by the following equation [40]:

$$I_r = AA^*T^2 \exp(-\frac{\Phi_{sc}}{k_B T})\exp(\frac{\beta_{sc}}{k_B T}(\frac{V}{d_s})^{0.5}) \; and \; I_r \tag{7}$$

and for the Poole–Frenkel effect

$$I_r = J_{LF} * \exp(\frac{\beta_{PF}}{kT}(\frac{V}{d_s})^{0.5}) \tag{8}$$

Fig. 13 shows the behavior of the Series Resistance R_s versus temperature for Au/POAP/TiO_2/p-Si/Al heterojunction diode. On the diagram the series resistance (R_S) decreases with an increase of temperature. The expression explaining the relationship between temperature and the concerned resistances is:

$$R_s = 2.0\,x10^9 exp(-0.057T) \tag{9}$$

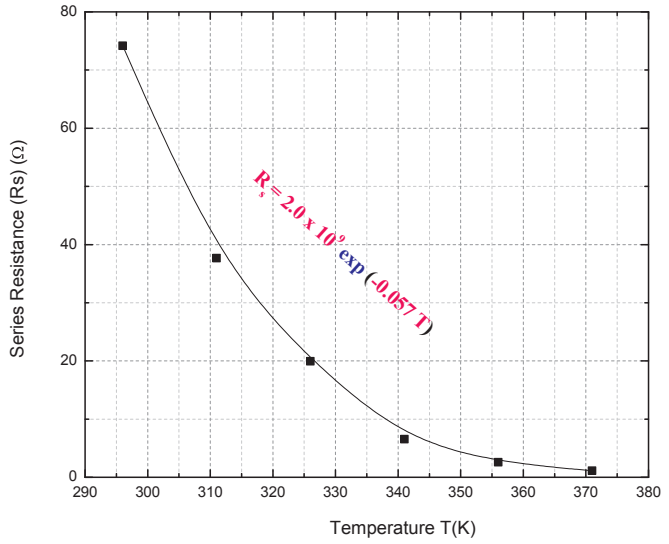

Fig. 13. Variation of series resistance versus temperature for Au/POAP/TiO_2/p-Si/heterojunction diode.

under the form

$$R_s = R_{s0} exp(B_s T) \tag{10}$$

where B_s is a coefficient specific to the semiconductor material ($B_s < 0$) and R_{s0} is the initial condition resistance [41].

3.6.2. Photovoltaic properties

Fig. 14 shows the evolution of the current versus voltage for Au/POAP/TiO_2/p-Si/Al heterojunction diode in dark and under the illumination intensity of 25, 50 and 75 W/m^2. The following equation provides the solar cell-diode parameters [42].

$$FF = V_M\, I_M / V_{OC}\, I_{SC} \tag{11}$$

The current and potential at maximum power point were expressed by I_M and V_M respectively. The following expression gives the maximum power given by the cell.

$$P_M = V_M\, I_M = FF \times V_{oc}\, I_{sc} \tag{12}$$

The experimental power conversion efficiency (PCE) of the solar cell (EES) is defined as.

$$PCE = P_M/P_{in} = [(FF.\, V_{OC.}\, J_{SC}/P_{in}) \times 100\%] \tag{13}$$

P_{in} is evaluated at 25, 50 and 75 W/m^2. The short current density by $J_{SC} = I_{SC}/A$. A being the cell active area. Figs. 15 and 16 exhibits the variation of current versus voltage characteristic of the maximum power section for Au/POAP/TiO_2/p-Si/Al heterojunction solar cell under illumination state. Photovoltaic factors of Au/POAP/p-Si/Al heterojunction solar cells at diverse illumination power are recorded in Table 4. The value of solar cells fills factor based on inorganic materials is higher than the present average fill factor value (FF = 0.15). However, the obtained average value of experimental power conversion efficiency (PCE) is 4.28%. The results presented in Table 5 designate that efficiency of the solar cells be influenced by the type of material utilized for light harvesting and type of formed junction (homojunction and heterojunction). The field dependent nature of the charge photogeneration process or high series resistance of the organic layer could be the essential reason of this effect.

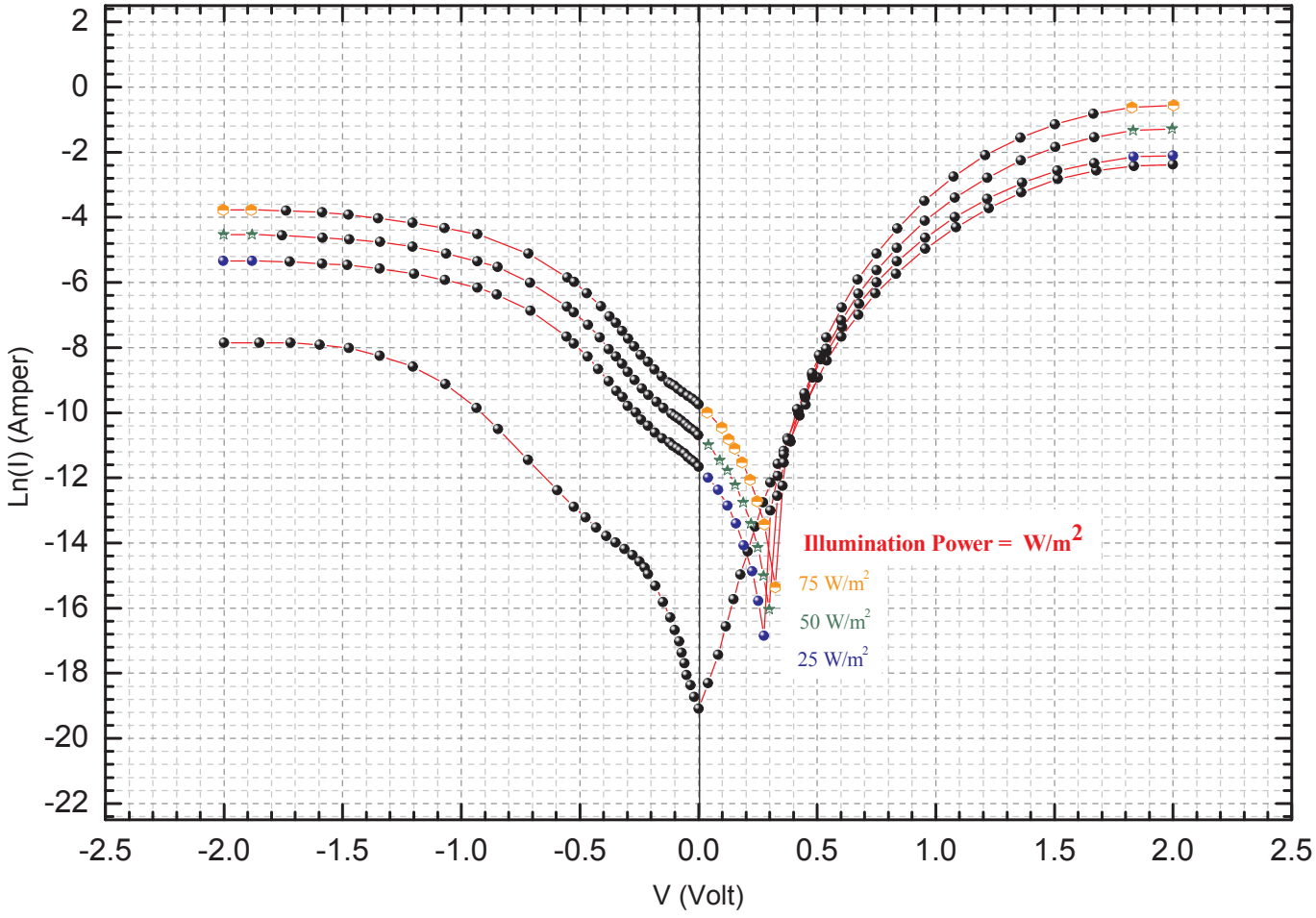

Fig. 14. Evolution of the current versus voltage for Au/POAP/TiO_2/p-Si/Al heterojunction diode.

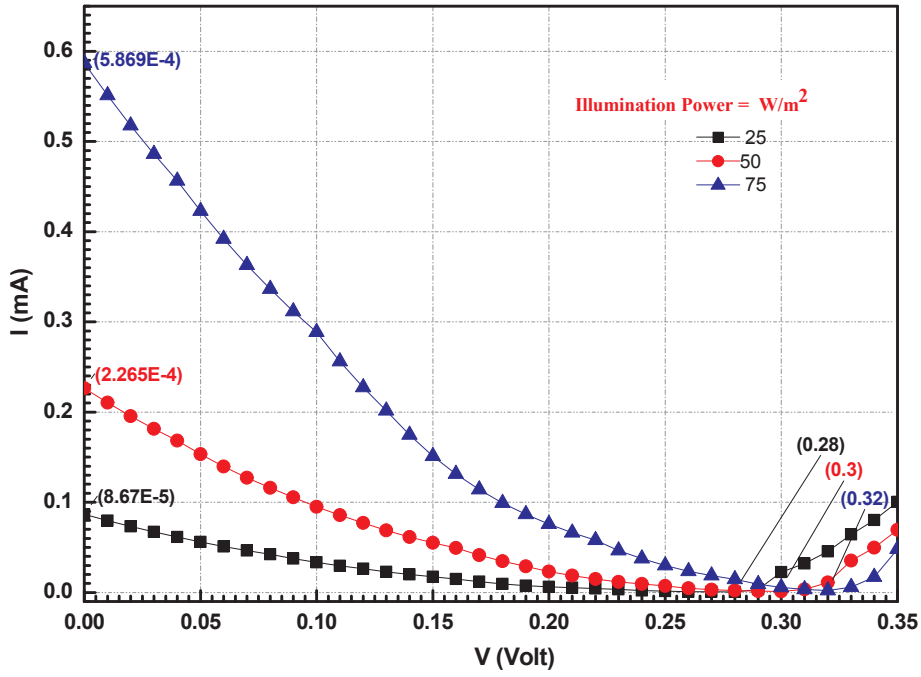

Fig. 15. Variation of the current versus voltage for Au/POAP/TiO_2/p-Si/Al heterojunction solar cell.

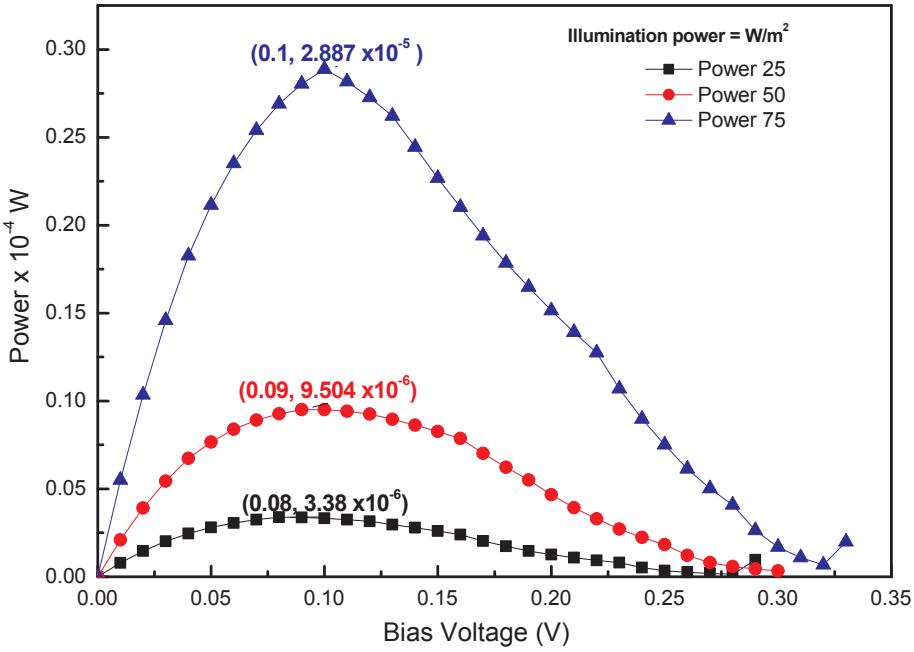

Fig. 16. Variation of the Bias voltage (V) versus power for Au/POAP/TiO_2/p-Si/Al heterojunction solar cell.

Table 4
Photovoltaic parameters of Au/POAP/p-Si/Al heterojunction solar cells.

Illumination power	V_M	I_M	V_{oc}	I_{sc}	FF	PCE
25	0.08	4.23E-05	0.28	8.67E-05	0.139	1.50
50	0.09	1.06E-04	0.3	2.27E-04	0.140	2.12
75	0.1	2.89E-04	0.32	5.87E-04	0.154	4.28

Table 5
Parameters of some organic solar cells.

Solar Cell Construction	V_{oc}	J_{sc}	FF	PCE	Refs
PET/PANI:CNT	0.73	68.5	0.45	2.27	[42]
P3HT/PCBM	0.61	106	0.67	4.37	[43]
ITO/PEDOT:PSS	0.60	21	0.41	5.40	[43]
Au/TPP/p-Si/Al	0.297	27.60	0.37	2.45	[44]
Au/POAP/p-Si/Al	0.32	6.52	0.15	4.28	Present work

TPP = tetraphenylporphyrin, PET substrates like PET, PANI polyaniline. CNT carbon nanotubes. P3HT/PCBM = poly(3-hexylthiophene): 6,6-phenyl-C61-butyric acid methyl ester. PEDOT: PSS = poly(3.4- ethylene dioxy thiophene) and poly(styrene sulfonate).

4. Conclusions

Hydrochloric acid doped-poly (o-aminophenol) with ladder-type structure was synthesized using a modified chemical oxidative polymerization method. The energy gaps of doped -poly (o-aminophenol) in thin film and in DMSO solution are found to be 2.454 eV and 2.641 eV respectively. The doped-poly (o-aminophenol) exhibits polydisperse and smooth particles with microstructure. The doped-poly (o-aminophenol) thin film has crystallinity nature. Au/POAP/TiO_2/p-Si/Al was fabricated as planar heterojunction for solar cell applications. Photovoltaic characteristics of under different intensities revealed that the thin film exhibited a PCE of ≅ 4.28% with an average filling factor of 0.15. Based on the promise PCE value, the efficiency of the solar cell can be enhanced by increasing the absolute temperature of the film layers.

Nomenclature

d	Interplanar spacing
E_g	Band gap
e	Activation energy
FF	Filling factor
$h\nu$	Photon energy
h, k, l	Miller indices
I	Junction current
I0	Reverse saturation current
Isc	Short circuit current
K_B	Boltzmann constant
JLF	Lower-field current density
n	Diode quality factor
Pin	Illumination intensity impinging on the cell
Rs	Series resistance
Rsh	Shunt resistance
RJ	Diode junction resistance
T	Temperature
φb	Barrier height
V	Voltage
Voc	Open circuit voltage
α	Absorption coefficient
α_o	Constant
β_{PF}	Poole–Frenkel field-lowering coefficient
β_{sc}	Schottky field-lowering coefficient
Φ_{sc}	Schottky depletion height

References

[1] V.D. Ivanov, D.V. Zhuzhel'skii, V.V. Malev, Comparison of properties of aniline and o-aminophenol polymers obtained using hydrogen peroxide, Russ. J. Electrochem. 44 (2008) 1204–1211.
[2] G. Bereket, B. Duran, Anticorrosive properties of electrosynthesized poly(m-aminophenol) on copper from aqueous phenylphosphonic acid solution, Prog. Org. Coating 64 (2009) 57–66.
[3] P. Kar, N.C. Pradhan, B. Adhikari, A novel route for the synthesis of processable conducting poly(m-aminophenol), Mater. Chem. Phys. 111 (2008) 59–64.
[4] P. Kar, N.C. Pradhan, B. Adhikari, Induced doping by sodium ion in poly(m-aminophenol) through the functional groups, Synth. Met. 160 (2010) 1524–1529.
[5] M. Sh. Zoromba, M.H. Abdel-Aziz, Ecofriendly method to synthesis poly (o-aminophenol) based on solid state polymerization and fabrication of nanostructured semiconductor thin film, Polymer 120 (2017) 20–29.

[6] T.C. Bicak, S. Soylemez, E. Buber, L. Toppare, Y. Yagci, Poly(o-aminophenol) prepared by Cu(II) catalyzed air oxidation and its use as a bio-sensing architecture, Polym. Chem. 26 (2017).
[7] N.M. Hosny, N. Nowesser, A.S. Al Hussaini, M. Sh. Zoromba, Solid state synthesis of hematite nanoparticles from doped poly o-aminophenol (POAP), J. Inorg. Organomet. Polym. 26 (2016) 41–47.
[8] D. Goncalves, R.C. Faria, M. Yonashiro, L.O.S. Bulhoes, Electrochemical oxidation of o-aminophenol in aqueous acidic medium: formation of film and soluble products, J. Electroanal. Chem. 487 (2000) 90.
[9] A.G. MacDiarmid, Alan G. MacDiarmid, "Synthetic metals": a novel role for organic polymers (Nobel lecture), Angew. Chem. Int. Ed. 40 (2001) 2581. Angewandte Chemie International Edition 40, no. 14 (2001) 2581–2590.
[10] J.E. Fromer, R.R. Chance, M. Grayson, J. Kroschwitz (Eds.), Encyclopedia of Polymer Science and Engineering, Wiley, New York, 1986, p. 462.
[11] C.K. Chiang, S.C. Gau, C.R. Fincher Jr., Y.W. Park, A.G. MacDiarmid, Polyacetylene, (CH) x: n-type and p-type doping and compensation, Appl. Phys. Lett. 33 (1978) 18–20.
[12] Q. Li, C. Zhang, J. Li, Photocatalysis and wave-absorbing properties of polyaniline/TiO 2 microbelts composite by in situ polymerization method, Appl. Surf. Sci. 257 (2010) 944–948.
[13] R. Gangopadhyay, A. De, Conducting polymer nanocomposites: a brief overview, Chem. Mater. 12 (2000) 608–622.
[14] A. Al-Bassam, Photoconductivity and defect levels in Zn x Cd 1 − x Se with (x = 0.5, 0.55) crystals, Sol. Energy Mater. Sol. Cell. 57 (1999) 323–329.
[15] W.R. Wu, C.J. Su, W.T. Chuang, Y.C. Huang, P.W. Yang, P.C. Lin, C.Y. Chen, T.Y. Yang, A.C. Su, K.H. Wei, Surface layering: surface layering and supersaturation for top-down nanostructural development during spin coating of polymer/fullerene thin films, Adv. Energy Mater. 7 (2017) 1601842.
[16] A.F. Al-Hossainy, A. Ibrahim, The effects of annealing temperature on the structural properties and optical constants of a novel DPEA-MR-Zn organic crystalline semiconductor nanostructure thin films, Opt. Mater. 73 (2017) 138–153.
[17] A.F. Al-Hossainy, H. Kh. Thabet, M. Sh. Zoromba, A. Ibrahim, Facile Synthesis and Fabrication of poly (ortho-anthranilic acid) emeraldine salt thin film for solar cells applications, New J. Chem. 42 (2018) 10386.
[18] M.K. Nazeeruddin, P. Pechy, T. Renouard, S.M. Zakeeruddin, R. Humphry-Baker, P. Comte, P. Liska, L. Cevey, E. Costa, V. Shklover, Engineering of efficient panchromatic sensitizers for nanocrystalline TiO2-based solar cells, J. Am. Chem. Soc. 123 (2001) 1613–1624.
[19] J.Y. Kim, S.H. Kim, H.H. Lee, K. Lee, W. Ma, X. Gong, A.J. Heeger, New architecture for high-efficiency polymer photovoltaic cells using solution-based titanium oxide as an optical spacer, Adv. Mater. 18 (2006) 572–576.
[20] I.M. Awad, F.S. Hassan, A.E. Mohamed, A.F. Al-Hossainy, Diphosphine compounds: part I. novel biologically active 1, 1′ bis-AND/OR 1, 2-cis-(Diphenylphosphino-) ethene and their complexes [M (CO) n {Ph2P (CHn) nPPh2}] & [Cu (Cl) 2 {Ph2P (CHn) nPPh2}], (M = W, Mo, Crn = 1, 2….n), Phosphorus, Sulfur, Silicon 179 (2004) 1251–1266.
[21] F.S. Hassan, A.F. Al-Hossainy, A.E. Mohamed, Diphosphine compounds, Part III: UV/visible spectroscopy and novel routes to functionalized diphosphine-M (CO) 6 complexes (M = W, Mo, or Cr), Phosphorus, Sulfur, Silicon 184 (2009) 2996–3022.
[22] C. Barbero, J.J. Silber, L. Sereno, Formation of a novel electroactive film by electropolymerization of ortho-aminophenol. Study of its chemical structure and formation mechanism. Electropolymerization of analogous compounds, J. Electroanal. Chem. 263 (1989) 333–352.
[23] O.A. El-Gammal, A.F. Al-Hossainy, S.A. El-Brashy, Spectroscopic, DFT, optical band gap, powder X-ray diffraction and bleomycin-dependant DNA studies of Co (II), Ni (II) and Cu (II) complexes derived from macrocyclic Schiff base, J. Mol. Struct. 1165 (2018) 177–195.
[24] A.F. Al-Hossainy, Synthesis, spectral, thermal, optical dispersion and dielectric properties of nanocrystalline dimer complex (PEPyr–diCd) thin films as novel organic semiconductor, Bull. Mater. Sci. 39 (2016) 209–222.
[25] M. Sh. Zoromba, M.H. Abdel-Aziz, M. Bassyouni, H. Bahaitham, A.F. Al-Hossainy, Poly (o-phenylenediamine) thin film for organic solar cell applications, J. Solid State Electrochem. (2018) 1–15.
[26] H. Xia, Q. Wang, Ultrasonic irradiation: a novel approach to prepare conductive polyaniline/nanocrystalline titanium oxide composites, Chem. Mater. 14 (2002) 2158–2165.
[27] G. Thenmozhi, P. Arockiasamy, R. Jaya Santhi, Isomers of poly aminophenol: chemical synthesis, characterization, and its corrosion protection aspect on mild steel in 1 M HCl, Int. J. Electrochem. (2014) 1–11. Article ID 961617.
[28] A. Badr, A. El-Amin, A. Al-Hossainy, Elucidation of charge transport and optical parameters in the newly 1CR-dppm organic crystalline semiconductors, J. Phys. Chem. C 112 (2008) 14188–14195.
[29] A. Elmansouri, A. Outzourhit, A. Lachkar, N. Hadik, A. Abouelaoualim, M.E. Achour, A. Oueriagli, E.L. Ameziane, Influence of the counter ion on the properties of poly(o-toluidine) thin films and their Schottky diodes, Synth. Met. 159 (2009) 292–297.
[30] R. Giovannetti, The use of spectrophotometry UV-vis for the study of porphyrins, Macro to Nano Spectroscopy, InTech, 2012.
[31] A.F. Al-Hossainy, M. Sh. Zoromba, R. Hassanien, Eco-friendly method to synthesize and characterize 2D nanostructured (1, 2-bis (diphenyl-phosphino) ethyl) tungsten tetracarbonyl methyl red/copper oxide di-layer thin films, Bull. Mater. Sci. 41 (2018) 80.
[32] A.T. Davidson, The effect of the metal atom on the absorption spectra of phthalocyanine films, J. Chem. Phys. 77 (1982) 162.
[33] A. Al-Hossainy, M.S. Zoromba, New organic semiconductor thin film derived from p-toluidine monomer, J. Mol. Struct. 1156 (2018) 83–90.
[34] T. Fujii, H. Nishikiori, T. Tamura, Absorption spectra of rhodamine B dimers in dip-coated thin films prepared by the sol-gel method, Chem. Phys. Lett. 233 (1995) 424–429.
[35] A. Badr, A. El-Amin, A. Al-Hossainy, Synthesis and optical properties for crystals of a novel organic semiconductor [Ni (Cl) 2 {(Ph 2 P) 2 CHC (R 1 R 2) NHNH 2}], Eur. Phys. J. B-Condens. Matter. Complex Syst. 53 (2006) 439–448.
[36] J. Bardeen, F.J. Slatt, L.T. Hall, Photoconductivity Conf vol. 146, Wiley, New York, 1965.
[37] S. Ambily, C.S. Menon, The effect of growth parameters on the electrical, optical and structural properties of copper phthalocyanine, Thin Solid Films 347 (1999) 284–288.
[38] M.M. El-Nahass, K.F. Abd-El-Rahman, A.A.M. Farag, A.A.A. Darwish, Photovoltaic properties of NiPc/p-Si (organic/inorganic) heterojunctions, Org. Electron. 6 (2005) 129–136.
[39] M.S. Sze, Physics of Semiconductor Devices, second ed., Wiley, New York, 1981.
[40] B. Tatar, A.E. Bulgurcuoglu, P. Gokdemir, P. Aydogan, D. Yılmazer, O. Ozdemir, K. Kutlu, Electrical and photovoltaic properties of Cr/Si Schottky diodes, Int. J. Hydrogen Energy 34 (2009) 5208–5212.
[41] S. Ashok, K.P. Pande, Photovoltaic measurements, Sol. Cell. 14 (1985) 61–81.
[42] R.V. Salvatierra, C.E. Cava, L.S. Roman, Aldo J.G. Zarbin, ITO-free and flexible organic photovoltaic device based on high transparent and conductive polyaniline/carbon nanotube thin films, Adv. Funct. Mater. 23 (2013) 1490–1499.
[43] G. Li, V. Shrotriya, J. Huang, Y. Yao, T. Moriarty, K. Emery, Y. Yang, High-efficiency solution processable polymer photovoltaic cells by self-organization of polymer blends, Nat. Mater. 4 (2005) 864–868.
[44] M.M. El-Nahass, H.M. Zeyada, M.s. Aziz, M.M. Makhlouf, Current transport mechanisms and photovoltaic properties of tetraphenylporphyrin/n-type silicon heterojunction solar cell, Thin Solid Films 492 (2005) 290–297.